investigations into the intracellular mechanisms for gene expression have been acquiring great importance [1]. Many cationic polymers indeed condense plasmid DNA (pDNA) through an electrostatic interaction, which is a requirement for effective cellular uptake [2,3]. However, sufficient transfection efficiency for clinical application has not been achieved, probably due to barriers such as endosomal degradation of pDNA or the limitation of nuclear localization. In recent years, special attention has been directed toward polyethylenimine (PEI), which has shown excellent gene expression compared with other polymers such as poly(L-lysine) (PLL). The mechanisms are usually explained by the 'proton-sponge' effect based on the uniqueness of the chemical structure of PEI [4,5]. Due to the integrated amino groups in the backbone structure, PEI possesses a low pKa to show a buffering property below physiological pH. Thus, PEI in the endosome interferes with pH lowering of the compartment, and induces an increased ion osmotic pressure to cause endosomal swelling and subsequent disruption [6]. Consequently, the endocytosed PEI polyplex can be efficiently delivered into the cytoplasm.

Two different structures of PEI, i.e., linear and branched PEI, have so far been applied to construct polyplex systems. Initially, appreciable gene expressions without using chloroquine were often reported for polyplexes composed of 800 and 25 kDa branched PEI (BPEI) [4,5,7–10], yet recent studies revealed that the 22 kDa linear PEI (LPEI) has even higher transfection activity [11–17]. Although BPEI and LPEI have identical chemical formulas, their buffering capacities are not considered comparable because of the difference in the amine composition: The amines present in LPEI are all secondary, in contrast, of those in BPEI, 25, 50, and 25% are primary, secondary, and tertiary, respectively [18]. Based on the studies comparing various LPEI and BPEI samples with a broad range of molecular weight, there were indeed observed significant differences in the transfection efficiencies [19,20]. Nevertheless, it is still unsolved whether the different efficiencies of the PEI family can simply be explained from the standpoint of the 'proton-sponge' effect, motivating us to conduct the present study to explore the intracellular behavior of PEI/pDNA polyplexes with varying composition.

Herein, we observed the intracellular fate of the internalized polyplexes by microscopic observation using fluorescently labeled pDNA. By using doubly labeled pDNA with a pair of donor–acceptor fluorescent dyes (fluorescein and Cy3), the condensation state of pDNA inside the cells was clearly detected by fluorescence resonance energy transfer (FRET) measurement. Moreover, the structural properties of the PEI/pDNA polyplexes, which might correlate with their intracellular kinetics, were analyzed by atomic force microscopy (AFM). Notably, in the LPEI/pDNA polyplexes, rapid escape from the endosomes, effective release of pDNA from the complex into the cytoplasm, and easy pDNA decondensation were observed in a sequential manner, correlating with the excellent and earlier detectable gene expression.

Materials and methods

Materials

Branched polyethylenimine (BPEI, MW 25 kDa) was purchased from Aldrich Chemical Co. (USA). Linear polyethylenimine (LPEI, MW 22 kDa) was purchased from MBI Fermentas (Exgen 500; Germany). Poly(L-lysine) (PLL, MW 53 900) and poly(aspartic acid) sodium salt (MW 26 000) were purchased from Sigma (St. Louis, MO, USA). The pDNA encoding luciferase (pGL3-Luc, Promega, USA; 5256 bps) was amplified in competent DH5α *Escherichia coli* and purified using EndoFree™ Plasmid Maxi Kits (Qiagen GmbH, Germany). The DNA concentration was determined by the absorbance at 260 nm. Dulbecco's modified Eagle's medium (DMEM) and fetal bovine serum (FBS) were purchased from Sigma. Texas Red Dextran (MW 3000) was purchased from Molecular Probes (Eugene, OR, USA). Hoechst 33258 was purchased from Dojindo (Japan).

Fluorescent labeling

The plasmid DNA (pDNA) was labeled in a similar way as that previously described using a Label IT nucleic acid labeling kit (Panvera, USA) [21]. Following a protocol provided by the manufacturer, slightly modified to allow double labeling of DNA, 5–50 μl of a pDNA solution (1 mg/ml) and the same amount of Label IT reagent (for fluorescein, Cy3 and X-rhodamine) were mixed in 20 mM MOPS buffer (pH 7.5) and incubated at 37 °C for 2 h. For double labeling, the two reagents (fluorescein + Cy3 or fluorescein + X-rhodamine) were simultaneously added to the pDNA solution. Any unreacted labeling reagent was removed and pDNA was purified by ethanol precipitation.

Preparation of polyplexes

The polycations and pDNA were separately dissolved in 10 mM Tris-HCl buffer (pH 7.4). Both solutions were mixed at various charge ratios of the number of nitrogen atoms to DNA phosphates. The final DNA concentration was adjusted to 33.3 μg/ml. After 15 min of incubation, the mixture was used for transfection and other measurements.

In vitro transfection

293T cells were seeded in 24-well culture plates. After a 24-h incubation in medium containing 10% FBS, the cells were rinsed and then 250 μl of culture medium without FBS were added to each well. Polyplex solution (25 μl; the pDNA concentration was 30μg/ml) was applied to each well. After 4 h, the medium was removed and replaced by 10% FBS containing medium for further incubation. The luciferase gene expression was measured using Fluoroscan Ascent FL (Dainippon, Japan).

Flow cytometric analysis

The polyplexes loaded with fluorescein-labeled pDNA were applied to the 293T cells in a manner similar to the procedure for *in vitro* transfection. After a 1-h incubation, the culture medium was aspirated and the cells were washed twice with phosphate-buffered saline (PBS). After detachment by pipetting and resuspension in PBS, the cells were analyzed using a flow cytometer (EPICS XL, Beckman Coulter, Inc.). Mock transfection allowed the definition of the natural fluorescence limit for the 293T cells and thus assessment of the fluorescein-positive cells. The cytometric data were analyzed using EXPO32™ software (Beckman Coulter, Inc.).

Laser confocal microscopy

The cells were seeded in 35-mm glass base dishes (Iwaki, Japan) for laser confocal analysis. A LSM 510 laser scanning microscope, set up from an Axiovert 100M microscope (Carl Zeiss, Germany), was used for the optical sectioning of the cells. An argon/krypton mixed gas laser with an excitation wavelength at 488 nm was used to induce emission from fluorescein and Cy3. For observation of the nuclei stained by Hoechst 33 258 and the endosomes stained by Texas Red Dextran, excitation wavelengths at 364 nm (Ar laser) and 543 nm (HeNe laser) were used, respectively.

When the pDNA was labeled with only fluorescein, the emission was observed using a 505 nm long pass filter. For analyzing FRET with doubly labeled pDNA, the emissions of fluorescein and Cy3 were detected by a 500–530 nm band pass filter and a 560 nm long pass filter, respectively. The fluorescence intensity ratios were calculated (LSM 510 Software, version 2.02; Carl Zeiss, Germany) at each pixel using the following equation:

$$\text{Fluorescein/Cy3 Ratio} = (S1 - S2)/(S1 + S2) \times 256 + 128$$

where S1 and S2 indicate the emission intensities of fluorescein and Cy3, respectively. The ratio image with an 8-bit (256 levels) gray scale was then created to express the ratios on the cell image.

Exchange reaction assay

The FRET measurements associated with the globule-to-coil transition of pDNA, which is triggered by the dissociation of the polyplexes, were carried out as previously described [21]. The fluorescence emission was measured at 25 °C using a spectrofluorometer (FP-777; JASCO, Japan). The excitation wavelength was 492 nm.

The LPEI, BPEI, and PLL/pDNA polyplexes (DNA concentration was 20 μg/ml) were prepared by using the doubly labeled (fluorescein and X-rhodamine) pDNA. After measurement of the initial emission intensity ratio of X-rhodamine/fluorescein, a 20% volume of poly(aspartic acid) solution (840 μg/ml) was added (the molar ratio of aspartic residue to DNA phosphate was 20), and, with gentle stirring, the time-dependent change in the emission intensity ratio was evaluated.

Atomic force microscopy

Each polyplex sample solution (5 μl) was deposited on a freshly cleaved mica substrate for 30 s. The solution was then rinsed with 50 μl of MilliQ deionized water (Millipore) and dried under a gentle flow of nitrogen gas. AFM imaging was performed in the tapping mode with standard silicon probes (Olympus, Tokyo, Japan) on a NVB100 microscope (Olympus) controlled by Nanoscope IIIa software (Digital Instruments, USA). The cantilever oscillation frequency was tuned to the resonance frequency of the cantilever, 260–340 kHz. The 256 × 256 images were recorded at a 0.5–2 μm/s linear scanning speed at a sampling density of 4–60 nm^2 per pixel. The raw AFM images were processed only for background removal (flattening) using the software.

Results

N/P ratio of cationic polymer/pDNA polyplexes

The polyplexes of the cationic polymers and pDNA at various N/P ratios (N/P = 1–20) were tested for transfection to 293T cells. The best transfection efficiencies were obtained for N/P = 10 in LPEI and BPEI, and N/P = 2 in PLL (data not shown). The gene expression obtained by LPEI was 10–100 times greater than BPEI (see Figure 6, discussed later). These N/P ratios were then used when preparing each polyplex throughout this study.

Transfer of the polyplexes from endosomes to the cytoplasm

The first step in the transfection is the cellular association and internalization of the polyplexes. By using the fluorescein-labeled pDNA, the cellular uptake of the polyplexes (LPEI, BPEI, and PLL/pDNA) was investigated. From flow cytometric analysis, the fluorescein-positive cells were estimated to be more than 90% even after a 1-h incubation with each polyplex, indicating that considerable association of these polyplexes and cells was achieved. The internalization of the polyplexes was then observed using laser confocal microscopy. To certify the escape from the endosomes, Texas Red Dextran was used as the endosome marker. After a 4-h incubation with either the LPEI/pDNA or the BPEI/pDNA polyplex, signals of fluorescein and Texas Red were separately observed in the cytoplasm (Figure 1), indicating that the polyplexes had already escaped from the endosomes. On the other

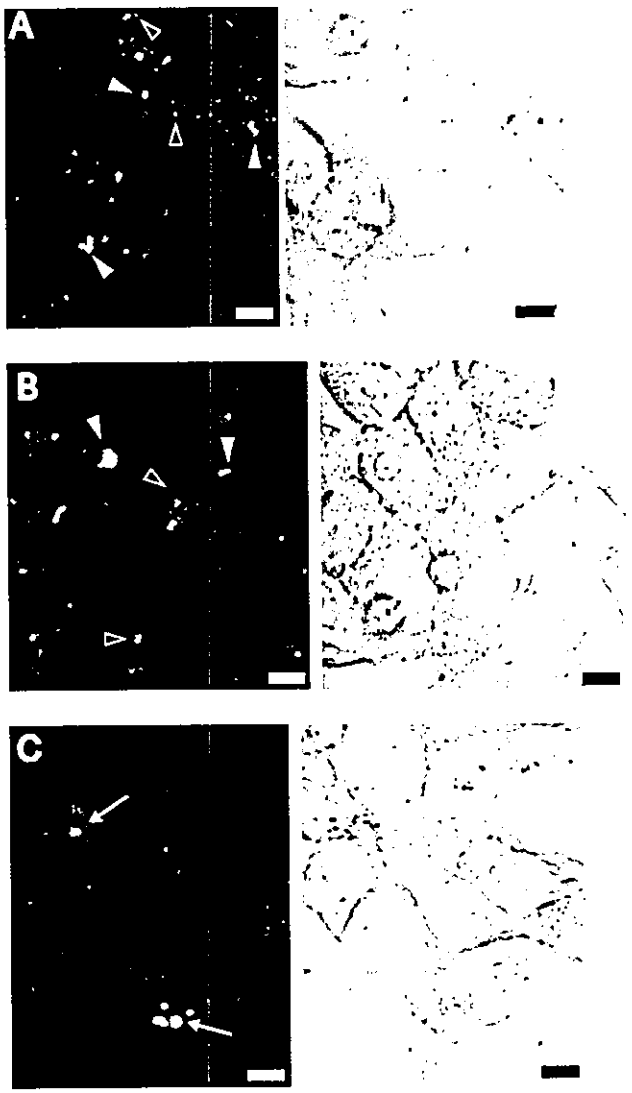

Figure 1. Transfer of the polyplexes from endosomes to the cytoplasm. The polyplexes were formed by polycations (LPEI, BPEI, and PLL) and fluorescein-labeled pDNA. 293T cells were seeded in 24-well culture plates. After a 24-h incubation in medium containing 10% FBS, the cells were rinsed and then 250 μl of culture medium without FBS were added to each well. The polyplex solution (25 μl; pDNA concentration was 30 μg/ml) was applied to each well. After a 4-h incubation, confocal microscopic images were obtained with endosome staining by Texas Red Dextran. The fluorescent images are shown on the left-hand side and the corresponding phase contrast images are on the right. (A) LPEI/pDNA and (B) BPEI/pDNA. DNA complexes (arrowhead) and dextran (open arrowhead) were separately observed. (C) PLL/pDNA. DNA complex and dextran were co-localized (observed as yellowish spot). Bar: 10 μm

hand, in the PLL/pDNA polyplexes, both the fluorescein and Texas Red signals were co-localized (observed as yellowish spot in Figure 1), even after 4 h.

It has been reported in the literature that the escape of BPEI/pDNA polyplexes from the endosomes occurs within 4 h after transfection based on an experiment using a proton pump inhibitor that prevented acidification of the endosomes [22]. In this study, both LPEI and BPEI were observed to escape from the endosomes after 4 h, presumably suggesting a similar endosomolytic activity of PEI by the proton-sponge effect.

Observation of pDNA decondensation in the cytoplasm

The next step for gene expression is pDNA release into the cytoplasm and transportation to the nucleus. After 24 h of transfection with the fluorescein-labeled pDNA, the microscopic images showed remarkable differences among the polyplexes. In LPEI/pDNA, the fluorescein signals were spread all around the cytoplasm (Figure 2). In contrast, the BPEI/pDNA polyplex was also distributed in the cytoplasm; however, it remained dot-shaped, similar to that observed after 1 h of transfection. This result suggested a difference in the polyplex structures.

For further investigation, the doubly labeled pDNA was used for FRET analysis. As previously reported, the condensation of the doubly labeled (fluorescein and X-rhodamine) pDNA in the polyplex induced FRET between the two fluorescent molecules, and the condensation state

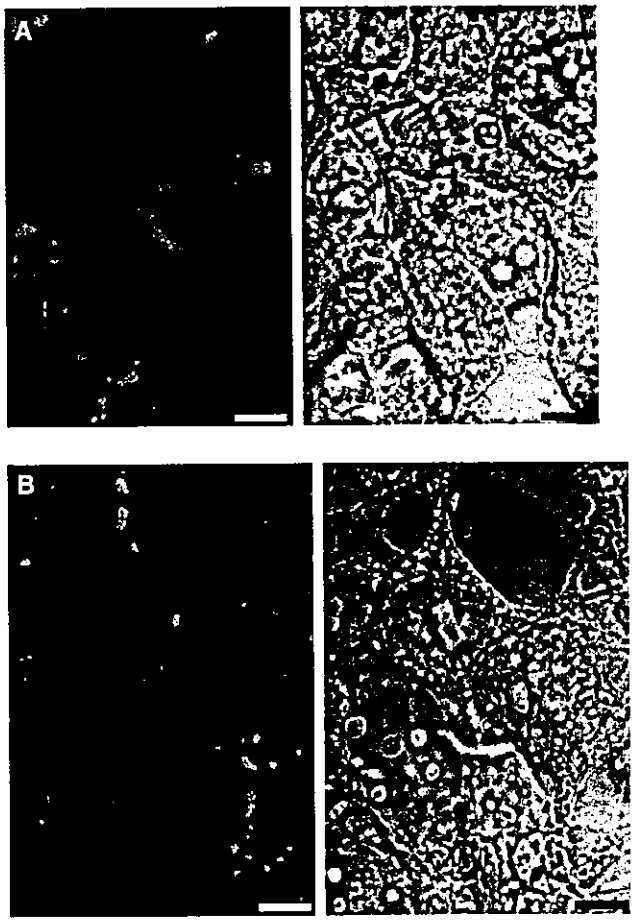

Figure 2. Intracellular distribution of fluorescein-labeled pDNA after 24 h of transfection. The polyplexes loaded with fluorescein-labeled pDNA were applied to the 293T cells. After a 24-h incubation, confocal microscopic images were obtained. The corresponding phase contrast images are on the right. (A) LPEI/pDNA and (B) BPEI/pDNA. Bar 10 μm

of pDNA can be evaluated even under physiological conditions [21]. In this study, fluorescein and Cy3 were used for double labeling. By spectral analysis with excitation at 492 nm, fluorescein (520 nm) has higher intensity than Cy3 (570 nm) in free pDNA. In contrast, when pDNA took a condensed state through complexation with the polycation, the emission peak of Cy3 significantly increased due to FRET from fluorescein, with a concomitant decrease in peak intensity of fluorescein (data not shown).

By using this doubly labeled pDNA, the intracellular distribution of polyplexes was analyzed by FRET under laser confocal microscopy. As shown in Figure 3, the cells transfected by the LPEI/pDNA polyplexes were observed with diffuse distribution of white-colored (higher value of the fluorescein/Cy3 ratio) pDNA in the cytoplasm. This higher fluorescein/Cy3 ratio compared with the background indicated that the emission intensity of fluorescein had higher emission intensity than Cy3 ($S1 > S2$; see 'Methods'), thus the pDNA acheived a decondensed state where FRET did not occur. In contrast, the cells transfected by the BPEI/pDNA polyplexes were observed as black-colored (lower fluorescein/Cy3 ratio; $S1 < S2$) and dotted particles, in which the pDNA remained in the condensed state (Figure 3). The result obtained by the PLL/pDNA polyplexes also indicated a similar condensation state. However, the number of polyplexes observed in the cytoplasm was extremely small, even lower compared with that observed after 4 h of transfection.

The DNA decondensation should be necessary to accomplish transcription to mRNA. The feasibility of the pDNA decondensation is thus believed to be closely correlated to the transfection efficiency. To confirm this hypothesis, the time-dependent increase in the pDNA decondensation and the gene expression was evaluated. In the LPEI/pDNA polyplexes, the intracellular decondensation of pDNA was observed within 4 h after transfection, and the amount of decondensed pDNA increased in a time-dependent manner (Figure 4). Concomitantly, the luciferase gene expression was confirmed as quickly as 4 h after transfection, and showed a time-dependent increase (Figure 5), thus presenting a clear correlation with the pDNA decondensation. In contrast, the gene expression by BPEI/pDNA was hardly observed after 4 h, which is consistent with the restricted pDNA decondensation, and, even after a 24-h incubation, only 1/50 to 1/100 of the gene expression was obtained.

It should be noted that pDNA transportation to the nucleus, where the transcription is considered to occur, was not clearly observed for any cases. As shown in Figures 3A and 4, the nucleus was observed as a 'punched-out' shape in the cell. After staining the nucleus with Hoechst 33 258, the localization of the fluorescein-labeled pDNA at the nucleus was rarely detected in each polyplex (Figure 6). Thus, there was a strong indication that only a small portion of the internalized pDNA had been transported to the nucleus. This issue may be related to the intracellular mobility of the polyplexes, and will be discussed below.

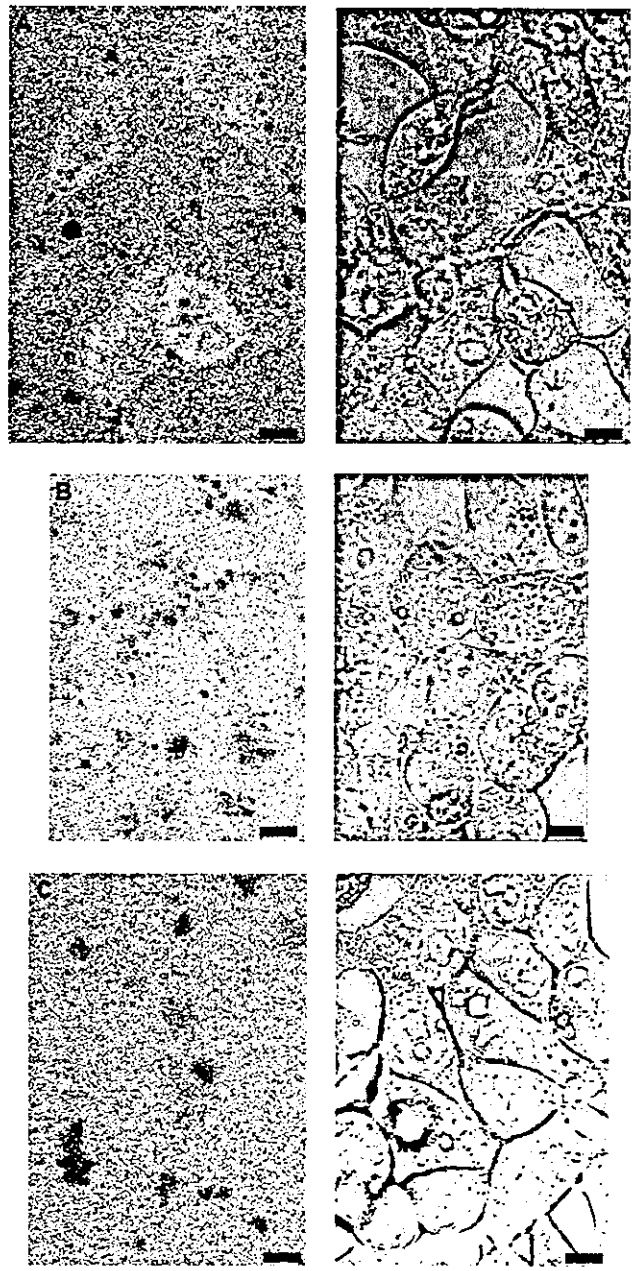

Figure 3. Polyplex distribution after 24 h of transfection expressed by the ratio images. The polyplexes loaded with doubly labeled (fluorescein and Cy3) pDNA were used. For analyzing FRET, the emissions of fluorescein and Cy3 were detected by a 500–530 nm band pass filter and a 560 nm long pass filter, respectively. The fluorescence intensity ratios were calculated at each pixel using LSM 510 Software version 2.02 (Carl Zeiss, Germany, see 'Methods'), and the ratio image with an 8-bit (256 levels) gray scale was then created to express the ratios on the cell image. The corresponding phase contrast images are on the right. (A) LPEI/pDNA; (B) BPEI/pDNA; and (C) PLL/pDNA. Bar 10 μm

Feasibility of the pDNA release from the polyplexes

The decondensation of pDNA is induced after pDNA dissociation from the polycation. Inside the cells, the

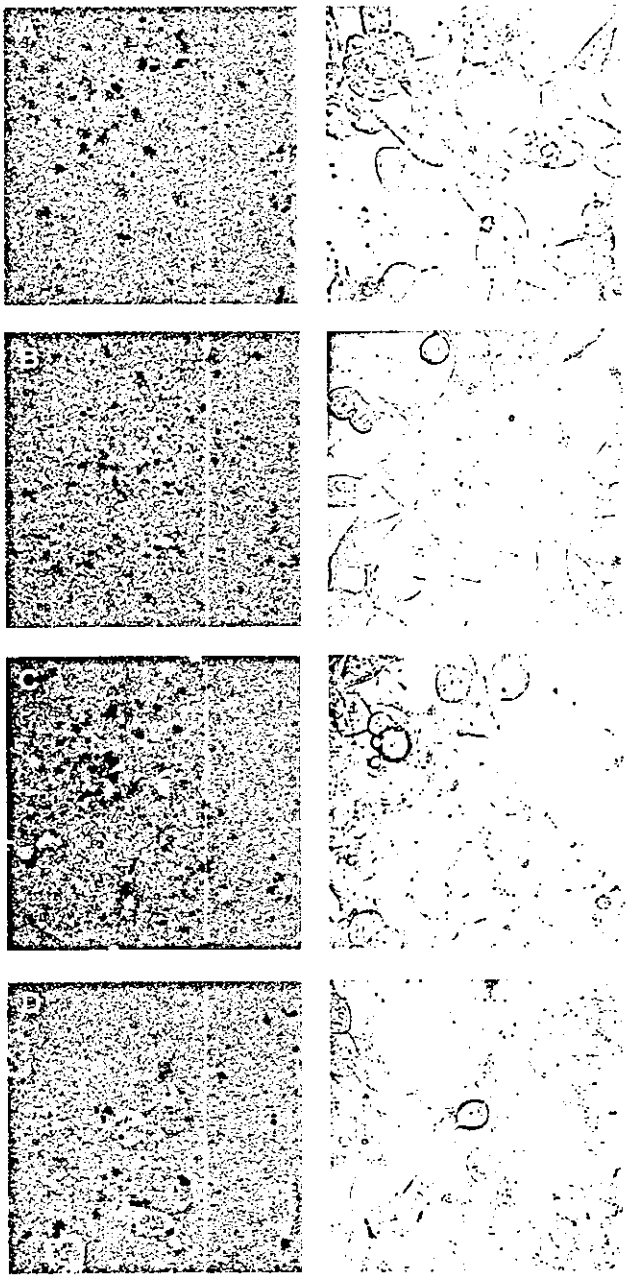

Figure 4. Time-dependent increase of decondensed pDNA after transfection with LPEI/pDNA polyplexes. The ratio images were created after transfection by LPEI/doubly labeled (fluorescein and Cy3) pDNA. The cells were observed with a diffuse distribution of white-colored (higher value of the fluorescein/Cy3 ratio) pDNA in the cytoplasm. This higher fluorescein/Cy3 ratio compared with the background indicated that the emission intensity of fluorescein had higher emission intensity than Cy3 (S1 > S2; see 'Methods'), thus the pDNA took a decondensed state where FRET did not occur. The corresponding phase contrast images are on the right. The ratio image after (A) 4 h; (B) 8 h; (C) 16 h; and (D) 24 h of transfection

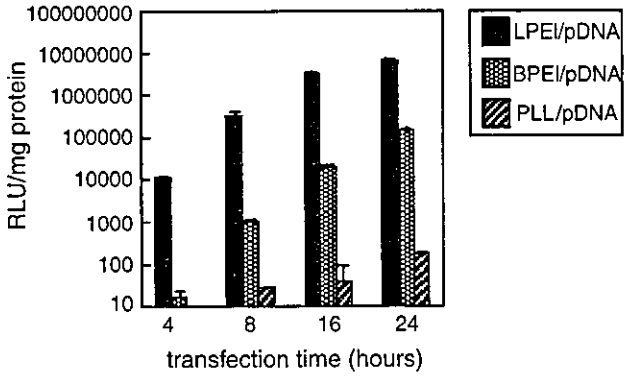

Figure 5. Time-dependent increase of luciferase gene expression with LPEI/pDNA, BPEI/pDNA, and PLL/pDNA polyplexes. After 4–24 h of transfection, the luciferase gene expression was measured using Fluoroscan Ascent FL (Dainippon, Japan). n = 6; ±SE

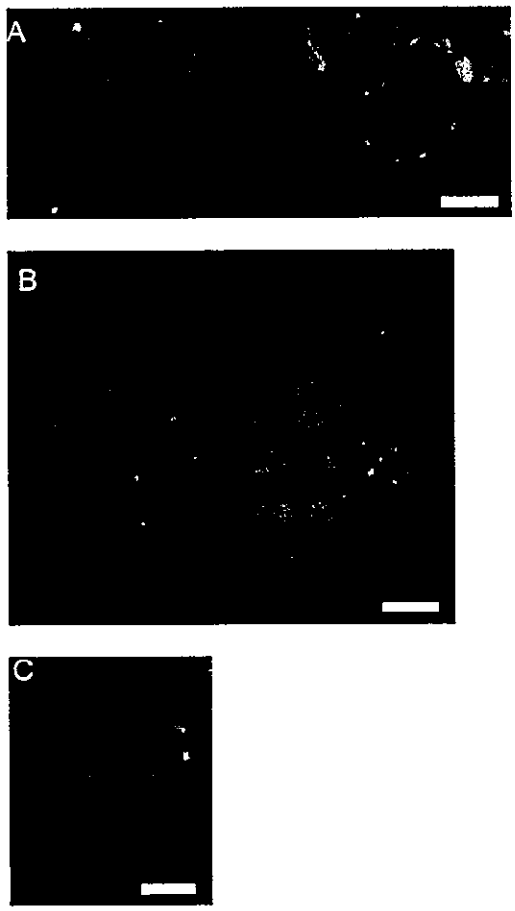

Figure 6. Fluorescent images after 24 h of transfection using fluorescein-labeled pDNA. The nucleus was stained with Hoechst 33258 prior to confocal microscopy for 15 min. Transfection with (A) LPEI/pDNA; (B) BPEI/pDNA; and (C) PLL/pDNA. Bar 10 μm

dissociation is considered to take place by an interexchange reaction of the complexed pDNA with the surrounding polyanion, such as cytoplasmic mRNA, phosphatidylserine, or anionic proteoglycan [23]. Thus, the feasibility of this interexchange reaction may distinctly affect gene expression and should be evaluated from the standpoint of its physicochemical properties.

By using the doubly labeled (fluorescein and X-rhodamine) pDNA, the interexchange reaction between the polyanion and the complexed pDNA in the LPEI, BPEI, and PLL/pDNA polyplexes was evaluated by FRET measurement [21]. Poly(aspartic acid) was used as the model counter-polyanion [24]. As shown in Figure 7, the LPEI and BPEI/pDNA polyplexes showed a rapid decrease in the emission intensity ratios, indicating that the DNA decondensation was induced by the dissociation from polycations. In contrast, the ratio of the PLL/pDNA polyplex decreased in a much slower manner. The tight binding of PLL with pDNA, resulting in the restricted release of pDNA through a chain exchange reaction, may have a role in the lower gene expression compared with PEI. Nevertheless, the kinetics of the decreased emission intensity ratios was not significant between LPEI and BPEI.

From a different viewpoint, it is worth noting that BPEI/pDNA had a remarkably higher initial intensity ratio than LPEI/pDNA. Since the intensity ratio is considered to reflect the condensation degree of pDNA, the BPEI/pDNA polyplexes are likely to induce a denser condensation of pDNA. This was further demonstrated by AFM (Figure 8). The polyplex diameters of LPEI and BPEI/pDNA were in a similar range, around 100 nm. These diameters were also confirmed by dynamic light scattering measurements (data not shown). However, in the cross section, the LPEI/pDNA polyplex was observed to have a multi-peak profile. In contrast, the BPEI/pDNA polyplex showed a taller and single-peak profile, suggesting a higher molecular density at the core of the complex. These results suggested that BPEI might induce the denser condensation of pDNA inside the polyplexes, which was in line with the higher FRET ratio of BPEI/pDNA.

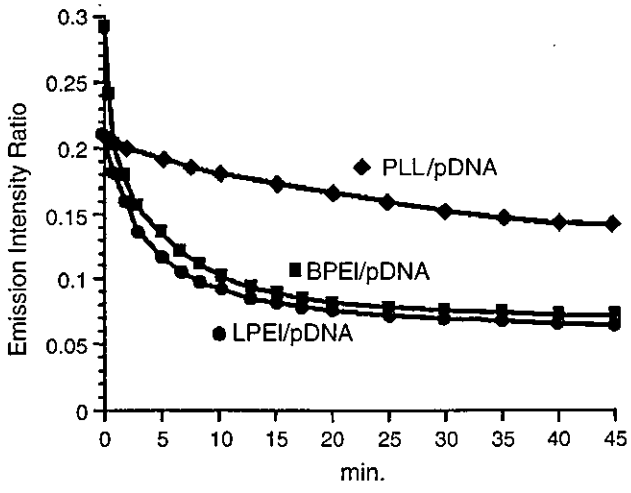

Figure 7. Interexchange reaction between poly(aspartic acid) and pDNA in the polyplexes. The LPEI, BPEI, and PLL/pDNA polyplexes were prepared by using the doubly labeled (fluorescein and X-rhodamine) pDNA. After measurement of the initial emission intensity ratio of X-rhodamine/fluorescein, poly(aspartic acid) solution was added, and, with gentle stirring, the time-dependent change of the emission intensity ratio was evaluated. (●) LPEI/pDNA; (■) BPEI/pDNA; and (♦) PLL/pDNA polyplexes

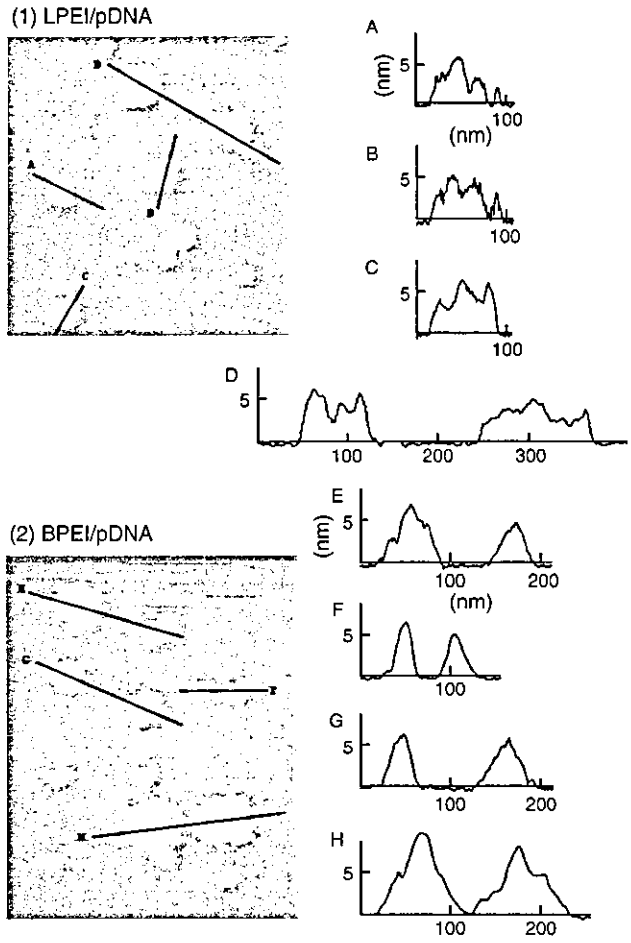

Figure 8. Atomic force microscopy of LPEI and BPEI/pDNA polyplexes. Each polyplex sample solution (5 μl) was deposited on a freshly cleaved mica substrate for 30 s. The solution was then rinsed with 50 μl of MilliQ deionized water (Millipore) and dried under a gentle nitrogen gas flow. AFM imaging was performed in the tapping mode with standard silicon probes (Olympus, Tokyo, Japan) on a NVB100 microscope (Olympus) controlled by Nanoscope IIIa software (Digital Instruments, USA). The cantilever oscillation frequency was tuned to the resonance frequency of the cantilever, 260–340 kHz. The 256 x 256 images were recorded at a 0.5–2 μm/s linear scanning speed at a sampling density of 4–60 nm^2 per pixel. The raw AFM images were processed only for background removal (flattening) using the software. (1) LPEI/pDNA and (2) BPEI/pDNA. The figures on the right are the cross sections at the lines indicated in the left-hand pictures (A–H)

Discussion

The process of transfection with non-viral gene delivery systems consists of many steps, such as the association of the DNA-loaded complexes with the cell surface, the internalization presumably by endocytosis, the escape from the endosomes, transport of the complexes or the released pDNA to the nucleus, and transcription in the nucleus. Each step may be a barrier to gene expression; however, the escape from the endosomes has been considered as one of the crucial obstacles. In this regard, PEI has been a promising candidate due to its buffering capacity under physiological pH conditions,

which is expected to induce endosomal rupture and enable polyplexes to escape without degradation. In fact, Akinc *et al.* reported that by using the fluorescent-labeled DNA, the pH environment of DNA inside the cells was measured as less acidic when delivered by BPEI and LPEI compared with PLL [25]. In contrast, it was also reported that an increase in pH was not observed around the PEI/pDNA polyplexes even by using a similar labeling method [26]. This inconsistency may be partly due to the difference in the labeling target, i.e., the former labeled the pDNA molecules and the latter the polymers. It is likely that the dissociation of the pDNA and polymers induces the discrepancy in their pH environments; however, details of their intracellular fate remain unclear.

These problems led us to this study focusing on the dissociation of pDNA from a cationic polymer. When released from the complexes, the pDNA should be decondensed from the condensed state inside the polyplexes. In the doubly labeled pDNA, the conformational change leads to a change in the distance between the two fluorescent molecules attached to a single pDNA molecule. Thus, pDNA decondensation through polyplex dissociation should be detected by FRET measurement [21]. Moreover, since this measurement can be carried out under physiological conditions, it is feasible to apply it for single cell observations under fluorescence microscopy.

In this study it was revealed that escape from the endosomes, presumably via the proton-sponge effect, was observed in the LPEI and BPEI/pDNA polyplexes. However, despite their identical chemical formulas, LPEI and BPEI showed a remarkable difference in intracellular behavior. LPEI presented a rapid and efficient pDNA decondensation in the cytoplasm, which was clearly correlated with the earlier detectable gene expression. In contrast, the BPEI/pDNA polyplexes were observed to remain in the condensed state even after 24 h of transfection.

Regardless of the condensation state of the pDNA, most of the fluorescent-labeled pDNAs was observed in the cytoplasm, suggesting that only a small portion of the internalized pDNA was transported to the nucleus. This is consistent with the restricted mobility of the high molecular DNA in the cytoplasm as reported by Lukacs *et al.* [27]. Note that even a single molecule of DNA with an applicable conformation for the transcription can repeatedly produce the mRNA, playing a key role, in a time-dependent manner, in determining the amount of the synthesized protein. It is thus suggested that the rapid and excellent gene expression is correlated with the increase in the concentration of intra-cytoplasmic pDNA undergoing smooth decondensation.

The BPEI/pDNA polyplexes were observed to remain mostly complexed in the cytoplasm. A similar result was reported by Godbey *et al.* [28]. They showed that by microscopic observation of the intracellular trafficking of the BPEI/pDNA polyplexes using separately labeled DNA and BPEI, both pDNA and BPEI were observed co-localizing in the nucleus as well as in the cytoplasm. These observations suggested that a portion of the BPEI/pDNA polyplexes was transported to the nucleus; however, the polymer and pDNA still remained complexed. Such a complexed pDNA is obviously unfavorable for transcription. This excessive stabilization of BPEI/pDNA polyplexes may cause lower gene expression compared with LPEI.

From the standpoint of physicochemical properties, the interexchange kinetics of pDNA and poly(aspartic acid) did not reveal any difference between LPEI and BPEI. However, the FRET analysis and the observations by AFM indicated that their structures were obviously different. Compared with LPEI, the BPEI/pDNA polyplex showed the more condensed structure. Consequently, in the cytoplasm, pDNA dissociation from BPEI is likely to be more difficult and a more time-requiring process than from LPEI.

On the other hand, PLL made a striking contrast both in intracellular behavior as well as the interexchange reaction. After transfection, the PLL/pDNA polyplexes were mostly entrapped in the endosomes, presumably due to the lack of the proton-sponge effect. In addition, the feasibility of the pDNA dissociation from PLL was found to be much less than that of PEI, indicating that the PLL/pDNA polyplexes are, in a sense, too stable in the cells. These PLL properties are thought to cause the significantly lower transfection efficiency compared with PEI. However, we recently observed that, even by using the PLL-based polymer systems, the sufficiently long incubation in the presence of chloroquine could produce a significant enhancement in gene expression (unpublished data), suggesting that dissociation of pDNA from PLL may be accomplished by the longer incubation.

In conclusion, the superiority of LPEI as a polyplex component is considered to be the rapidity of gene expression due to the smooth intracellular disintegration of the complex with pDNA. This property may be particularly beneficial to achieve an appreciably high gene expression in a prompt manner.

Acknowledgements

This work was financially supported by Grants-in-Aid for Scientific Research (no. 11167210 to K.K and no. 12877221 to H.K.) and Special Coordination Funds for Promoting Science and Technology from the Ministry of Education, Culture, Sports, Science and Technology of Japan as well as by the Core Research Program for Evolutional Science and Technology (CREST) from the Japan Science and Technology Corporation (JST).

References

1. Han S, Mahato RI, Sung YK, Kim SW. Development of biomaterials for gene therapy. *Mol Ther* 2000; 2: 302–317.
2. Kabanov AV. Taking polycation gene delivery systems from in vitro to in vivo. *Pharm Sci Technol Today* 1999; 2: 365–372.
3. De Smedt SC, Demeester J, Hennink WE. Cationic polymer based gene delivery systems. *Pharm Res* 2000; 17: 113–126.
4. Boussif O, Lezoualc'h F, Zanta MA, *et al.* A versatile vector for gene and oligonucleotide transfer into cells in culture and

in vivo: polyethylenimine. *Proc Natl Acad Sci U S A* 1995; **92**: 7297–7301.
5. Boussif O, Zanta MA, Behr JP. Optimized galenics improve in vitro gene transfer with cationic molecules up to 1000-fold. *Gene Ther* 1996; **3**: 1074–1080.
6. Behr JP. The proton sponge: a trick to enter cells the viruses did not exploit. *Chimia* 1997; **51**: 34–36.
7. Abdallah B, Hassan A, Benoist C, Goula D, Behr JP, Demeneix BA. A powerful nonviral vector for in vivo gene transfer into the adult mammalian brain: polyethylenimine. *Hum Gene Ther* 1996; **7**: 1947–1954.
8. Kircheis R, Kichler A, Wallner G, *et al.* Coupling of cell-binding ligands to polyethylenimine for targeted gene delivery. *Gene Ther* 1997; **4**: 409–418.
9. Ogris M, Steinlein P, Kursa M, Mechtler K, Kircheis R, Wagner E. The size of DNA/transferrin-PEI complexes is an important factor for gene expression in cultured cells. *Gene Ther* 1998; **5**: 1425–1433.
10. Fischer D, Bieber T, Li Y, Elsasser HP, Kissel T. A novel nonviral vector for DNA delivery based on low molecular weight, branched polyethylenimine: effect of molecular weight on transfection efficiency and cytotoxicity. *Pharm Res* 1999; **16**: 1273–1279.
11. Ferrari S, Moro E, Pettenazzo A, Behr JP, Zacchello F, Scarpa M. ExGen 500 is an efficient vector for gene delivery to lung epithelial cells in vitro and in vivo. *Gene Ther* 1997; **4**: 1100–1106.
12. Goula D, Remy JS, Erbacher P, *et al.* Size, diffusibility and transfection performance of linear PEI/DNA complexes in the mouse central nervous system. *Gene Ther* 1998; **5**: 712–717.
13. Bragonzi A, Boletta A, Biffi A, *et al.* Comparison between cationic polymers and lipids in mediating systemic gene delivery to the lungs. *Gene Ther* 1999; **6**: 1995–2004.
14. Li S, Tan Y, Viroonchatapan E, Pitt BR, Huang L. Targeted gene delivery to pulmonary endothelium by anti-PECAM antibody. *Am J Physiol Lung Cell Mol Physiol* 2000; **278**: L504–L511.
15. Poulain L, Ziller C, Muller CD, *et al.* Ovarian carcinoma cells are effectively transfected by polyethylenimine (PEI) derivatives. *Cancer Gene Ther* 2000; **7**: 644–652.
16. Wightman L, Kircheis R, Rossler V, *et al.* Different behavior of branched and linear polyethylenimine for gene delivery in vitro and in vivo. *J Gene Med* 2001; **3**: 362–372.
17. Brunner S, Furtbauer E, Sauer T, Kursa M, Wagner E. Overcoming the nuclear barrier: cell cycle independent nonviral gene transfer with linear polyethylenimine or electroporation. *Mol Ther* 2002; **5**: 80–86.
18. Suh J, Paik H-J, Hwang BK. Ionization of poly(ethylenimine) and poly(allyamine) at various pH's. *Bioorg Chem* 1994; **22**: 318–327.
19. Godbey WT, Wu KK, Mikos AG. Size matters: molecular weight affects the efficiency of poly(ethylenimine) as a gene delivery vehicle. *J Biomed Mater Res* 1999; **45**: 268–275.
20. Gebhart CL, Kabanov AV. Evaluation of polyplexes as gene transfer agents. *J Control Release* 2001; **73**: 401–416.
21. Itaka K, Harada A, Nakamura K, Kawaguchi H, Kataoka K. Evaluation by fluorescence resonance energy transfer of the stability of nonviral gene delivery vectors under physiological conditions. *Biomacromolecules* 2002; **3**: 841–845.
22. Kichler A, Leborgne C, Coeytaux E, Danos O. Polyethylenimine-mediated gene delivery: a mechanistic study. *J Gene Med* 2001; **3**: 135–144.
23. Labat-Moleur F, Steffan AM, Brisson C, *et al.* An electron microscopy study into the mechanism of gene transfer with lipopolyamines. *Gene Ther* 1996; **3**: 1010–1017.
24. Katayose S, Kataoka K. Water-soluble polyion complex associates of DNA and poly(ethylene glycol)-poly(L-lysine) block copolymer. *Bioconjug Chem* 1997; **8**: 702–707.
25. Akinc A, Langer R. Measuring the pH environment of DNA delivered using nonviral vectors: implications for lysosomal trafficking. *Biotechnol Bioeng* 2002; **78**: 503–508.
26. Forrest ML, Pack DW. On the kinetics of polyplex endocytic trafficking: implications for gene delivery vector design. *Mol Ther* 2002; **6**: 57–66.
27. Lukacs GL, Haggie P, Seksek O, Lechardeur D, Freedman N, Verkman AS. Size-dependent DNA mobility in cytoplasm and nucleus. *J Biol Chem* 2000; **275**: 1625–1629.
28. Godbey WT, Wu KK, Mikos AG. Tracking the intracellular path of poly(ethylenimine)/DNA complexes for gene delivery. *Proc Natl Acad Sci U S A* 1999; **96**: 5177–5181.

ORIGINAL ARTICLE

Corneal Reconstruction with Tissue-Engineered Cell Sheets Composed of Autologous Oral Mucosal Epithelium

Kohji Nishida, M.D., Ph.D., Masayuki Yamato, Ph.D., Yasutaka Hayashida, M.D., Katsuhiko Watanabe, M.Sc., Kazuaki Yamamoto, M.Sc., Eijiro Adachi, M.D., Ph.D., Shigeru Nagai, M.Sc., Akihiko Kikuchi, Ph.D., Naoyuki Maeda, M.D., Ph.D., Hitoshi Watanabe, M.D., Ph.D., Teruo Okano, Ph.D., and Yasuo Tano, M.D., Ph.D.

ABSTRACT

BACKGROUND

Ocular trauma or disease may lead to severe corneal opacification and, consequently, severe loss of vision as a result of complete loss of corneal epithelial stem cells. Transplantation of autologous corneal stem-cell sources is an alternative to allograft transplantation and does not require immunosuppression, but it is not possible in many cases in which bilateral disease produces total corneal stem-cell deficiency in both eyes. We studied the use of autologous oral mucosal epithelial cells as a source of cells for the reconstruction of the corneal surface.

METHODS

We harvested 3-by-3-mm specimens of oral mucosal tissue from four patients with bilateral total corneal stem-cell deficiencies. Tissue-engineered epithelial-cell sheets were fabricated ex vivo by culturing harvested cells for two weeks on temperature-responsive cell-culture surfaces with 3T3 feeder cells that had been treated with mitomycin C. After conjunctival fibrovascular tissue had been surgically removed from the ocular surface, sheets of cultured autologous cells that had been harvested with a simple reduced-temperature treatment were transplanted directly to the denuded corneal surfaces (one eye of each patient) without sutures.

RESULTS

Complete reepithelialization of the corneal surfaces occurred within one week in all four treated eyes. Corneal transparency was restored and postoperative visual acuity improved remarkably in all four eyes. During a mean follow-up period of 14 months, all corneal surfaces remained transparent. There were no complications.

CONCLUSIONS

Sutureless transplantation of carrier-free cell sheets composed of autologous oral mucosal epithelial cells may be used to reconstruct corneal surfaces and can restore vision in patients with bilateral severe disorders of the ocular surface.

From the Department of Ophthalmology, Osaka University Medical School, Osaka (K.N., Y.H., K.W., K.Y., N.M., H.W., Y.T.); the Institute of Advanced Biomedical Engineering and Science, Tokyo Women's Medical University, Tokyo (M.Y., S.N., A.K., T.O.); and the Department of Molecular Morphology, Kitasato University Graduate School of Medicine, Kanagawa (E.A.) — all in Japan. Address reprint requests to Dr. Nishida at the Department of Ophthalmology, Osaka University Medical School, Room E7, Yamadaoka 2-2, Suita, Osaka 565-0871, Japan, or at knishida@ophthal.med.osaka-u.ac.jp.

N Engl J Med 2004;351:1187-96.

CORNEAL EPITHELIAL STEM CELLS RE-side in the basal layer of the limbus,[1,2] the transitional zone between the cornea and the bulbar conjunctiva. These cells govern renewal of the corneal epithelium[3] by generating progeny (transient amplifying cells, which are cells committed to epithelial differentiation) with limited renewal capabilities that migrate from the limbus into the basal layer of the cornea.[4]

If corneal epithelial stem cells are completely absent owing to limbal disorder from severe trauma (e.g., thermal or chemical burns) or eye diseases (e.g., the Stevens–Johnson syndrome or ocular pemphigoid), then the sources of corneal epithelial cells have been exhausted, the peripheral conjunctival epithelium invades inwardly, and the corneal surface becomes enveloped by vascularized conjunctival scar tissue, resulting in corneal opacification that leads to severe visual impairment. Such pathological characteristics are considered to represent limbal stem-cell deficiencies.[5,6]

In patients with unilateral limbal stem-cell deficiency, autologous limbal transplantation is a method of surface reconstruction of the cornea.[7] This procedure, however, requires a large limbal graft from the healthy eye (incurring a risk of causing limbal stem-cell deficiency in the healthy eye[8]), and it is not possible in patients who have bilateral lesions.[9]

Limbal-allograft transplantation can be performed in patients with unilateral or bilateral deficiencies,[10] but it requires long-term immunosuppression that involves high risks of serious eye and systemic complications including infection and liver and kidney dysfunction.[10] In patients with the Stevens–Johnson syndrome or ocular pemphigoid, graft failure is common, even with immunosuppression, owing to serious preoperative conditions such as persistent inflammation of the ocular surface, abnormal epithelial differentiation of the ocular surface, severe dry eye, and lid-related abnormalities.[11-13]

To avoid allograft rejection and improve surgical outcome, some patients with unilateral stem-cell deficiencies have had corneal epithelial grafts constructed ex vivo by the expansion of autologous limbal stem cells harvested from healthy contralateral eyes and cultivated on cell carriers such as amniotic membranes[14,15] and fibrin gel.[16] This process, however, cannot be used for bilateral total limbal stem-cell deficiencies. Therefore, we studied an alternative replacement strategy for damaged corneal epithelium involving a tissue-engineered epithelial-cell sheet comprising only the patient's own oral mucosal epithelial cells. Transplantation of autologous oral mucosal epithelial cells cultured on amniotic membranes to a rabbit corneal model has recently been reported.[17,18]

We studied a new method of transplantation involving a carrier-free cell sheet by exploiting temperature-responsive culture surfaces. By lowering the temperature, we are able to detach all the cultured cells from the surfaces as an intact transplantable cell sheet, and any carrier or scaffold is excluded from the graft.[19] We report the results of ocular-surface reconstruction in four patients with the use of cultured autologous oral mucosal epithelial cells and carrier-free tissue-replacement sheets.

METHODS

SUBJECTS

This study was approved by the institutional review board of Osaka University Medical School, in Osaka, Japan. Oral and written informed consent were obtained from all patients. Patients with bilateral total limbal stem-cell deficiency were eligible for inclusion. Exclusion criteria included glaucoma or xerophthalmia (a skinlike appearance) of the entire ocular surface. Our results are for the first four consecutive patients enrolled, each of whom had one eye grafted with a tissue-engineered epithelial-cell sheet fabricated in culture from harvested autologous oral mucosal epithelial cells in our hospital from January 2003 through March 2003 (Table 1).

All grafted eyes had been clinically diagnosed as having total limbal stem-cell deficiency with complete disappearance of the palisades of Vogt (a radial infolding at the sclerocorneal junction and a biologic marker of the location of corneal epithelial stem cells) and complete coverage by fibrovascular in-growth from 360 degrees of the limbus over the entire cornea. All patients exhibited chronic conjunctival inflammation immunologically driven by the causative diseases reported previously,[20,21] despite therapy with topical steroids. Three of the four patients (Patients 1, 3, and 4) had severe deficiency of the tear film. Lid abnormalities, including chronic blepharitis, misdirection of the eyelashes, and keratinization of the posterior lid margin, contributed to poor ocular-surface conditions and were also noted in all eyes. Patients 1 and 4 had continuous inflammation with severe tear-film and lid abnormalities and keratinization of the ocular

Table 1. Preoperative Characteristics of Patients with Total Limbal Deficiency.

Patient No.	Age	Sex	Diagnosis	Eye	Ocular-Surface Condition			Previous Surgery	Other Eye Diseases
					Symblepharon*	Schirmer's Test without Topical Anesthesia†	Schirmer's Test with Nasal Stimulation‡		
	yr					*mm*			
1	58	M	Stevens–Johnson syndrome (chronic phase)	Right	+	1	2	Allogeneic corneal epithelium (cultivated on amniotic membrane) transplantation in 2000	None
2	69	M	Ocular cicatricial pemphigoid	Left	+	23	26	None	None
3	77	F	Ocular cicatricial pemphigoid	Right	+	1	1	Limbal transplantation with the use of amniotic membrane in 2001	Proliferative diabetic retinopathy, branch-retinal-vein occlusion
4	75	F	Ocular cicatricial pemphigoid	Right	+	1	2	Penetrating keratoplasty in 1999	None

* The plus sign indicates that symblepharon (adhesion of one or both eyelids to the eyeball) was found at the patient's ocular surface.

† Schirmer's test without anesthesia is a commonly used clinical test of lacrimal secretion (tearing). It is performed by measuring the amount of moisture on Whatman filter paper (5 mm by 35 mm) that is placed in the margin of the lower lid for five minutes. A value of less than 5 mm indicates impaired secretion.

‡ Schirmer's test with nasal stimulation is used to measure maximal tearing and is performed by inserting a cotton swab into the nasal cavity. A value of less than 10 mm indicates decreased tearing.

surface. Three of the four patients (Patients 1, 3, and 4) had previously undergone allogeneic grafting, which had failed within one year after surgery, despite systemic and local immunosuppression with cyclosporine (trough levels of 50 to 100 ng per milliliter).

Surgical procedures for all cell-sheet autografts were performed by the same surgeon. A complete ophthalmologic examination included measurement of best corrected visual acuity, slit-lamp biomicroscopy, tonometry, and indirect ophthalmoscopy and was performed in all patients every two to four weeks during the follow-up period, starting two weeks after transplantation. The assessments of visual outcomes were carried out by investigators who were not involved in performing the procedures and were not informed about which eye underwent transplantation or whether the assessment was preoperative or postoperative.

CULTURE AND FABRICATION OF AUTOLOGOUS ORAL MUCOSAL EPITHELIAL-CELL SHEETS

After each patient's oral cavity was sterilized with topical povidone-iodine, a 3-by-3-mm specimen of oral mucosal tissue was surgically excised from the interior buccal mucosal epithelium while the patient was under local anesthesia with xylocaine (Fig. 1A). Oral mucosal epithelial cells were collected by removing all epithelial layers after treatment with dispase II (3 mg per milliliter, Roche), at 37°C for one hour. Collected materials were placed in trypsin and EDTA for 15 minutes to form single-cell suspensions. Temperature-responsive cell-culture inserts (CellSeed) were prepared with the use of commercial cell-culture inserts (Falcon, Becton Dickinson) according to specific procedures described previously.[22] The temperature-responsive polymer poly(*N*-isopropylacrylamide), which reversibly alters its hydration properties with temperature, is chemically immobilized in thin films on cell-culture surfaces, facilitating cell adhesion and growth in normal culture conditions at 37°C. Reducing the temperature of the culture below 30°C causes this surface to hydrate and swell rapidly, prompting complete detachment of adherent cells without the use of typical proteolytic enzymes or treatment with EDTA. Confluent cell cultures on these surfaces can be conveniently harvested as a single, unsupported contiguous cell sheet, retaining cell-to-cell junctions as well as deposited extracellular matrix on the basal surface of the sheet.[23] Enzyme-free harvest permits the cell sheets to be readily manipulated, transferred, layered, or fabricated, because they adhere rapidly to other surfaces, such as traditional culture plastics,[22] other cell sheets, and tissues in vivo.[19]

To prepare lethally treated feeder layers, subconfluent NIH 3T3 cells were incubated with 16 μg of mitomycin C per milliliter for two hours at 37°C and then trypsinized and seeded onto tissue-culture wells (35-mm diameter, Becton Dickinson) at a density of 2×10^4 cells per square centimeter. Oral epithelial cells were separated from these feeder-layer cells during culture with temperature-responsive cell-culture inserts. We confirmed that multilayered cell sheets were fabricated only in the presence of 3T3 cells in the culture system. After culture in vitro for 14 days, epithelial-cell sheets (23.4 mm in diameter) were harvested by reducing the temperature to 20°C.

For colony-forming assays, treatment with trypsin and EDTA was used to isolate single cells from oral mucosal epithelium. Cells were counted, seeded onto culture dishes (35-mm diameter, Becton Dickinson), and cultured with feeder layers treated with mitomycin C. After cultivation for 10 to 12 days, dishes were fixed and stained with rhodamine B. Colony formation in the entire dish was screened under a dissecting microscope.

Figure 1 (facing page). Transplantation of Autologous Tissue-Engineered Epithelial-Cell Sheets Fabricated from Oral Mucosal Epithelium.

Panel A shows the removal of oral mucosal tissue (3 by 3 mm) from patient's cheek. Isolated epithelial cells are seeded onto temperature-responsive cell-culture inserts. After two weeks at 37°C, these cells grow to form multilayered sheets of epithelial cells. The viable cell sheet is harvested with intact cell-to-cell junctions and extracellular matrix in a transplantable form simply by reducing the temperature of the culture to 20°C for 30 minutes. The cell sheet is then transplanted directly to the diseased eye without sutures. In Panel B (the scale bar represents 50 μm), harvested cell sheets have three to five cell layers and do not resemble the original oral mucosa as shown in Panel C (the scale bar represents 100 μm) as closely as they resemble normal corneal epithelium as shown in Panel D (the scale bar represents 100 μm). Panel E shows a transmission electron micrograph of developed microvilli on the apical surface of the cell sheet. Specimens of human tissue-engineered epithelial-cell sheets harvested by reducing the temperature of the culture are immunostained green with anti–keratin 3 antibodies (Panel F), anti-β_1 integrin antibodies (Panel G), and anti-p63 antibodies (Panel H). The nuclei in Panels F, G, and H are shown in red. The scale bars represent 50 μm in Panels F, G, and H. The specimens in Panels B, C, and D are stained with hematoxylin and eosin.

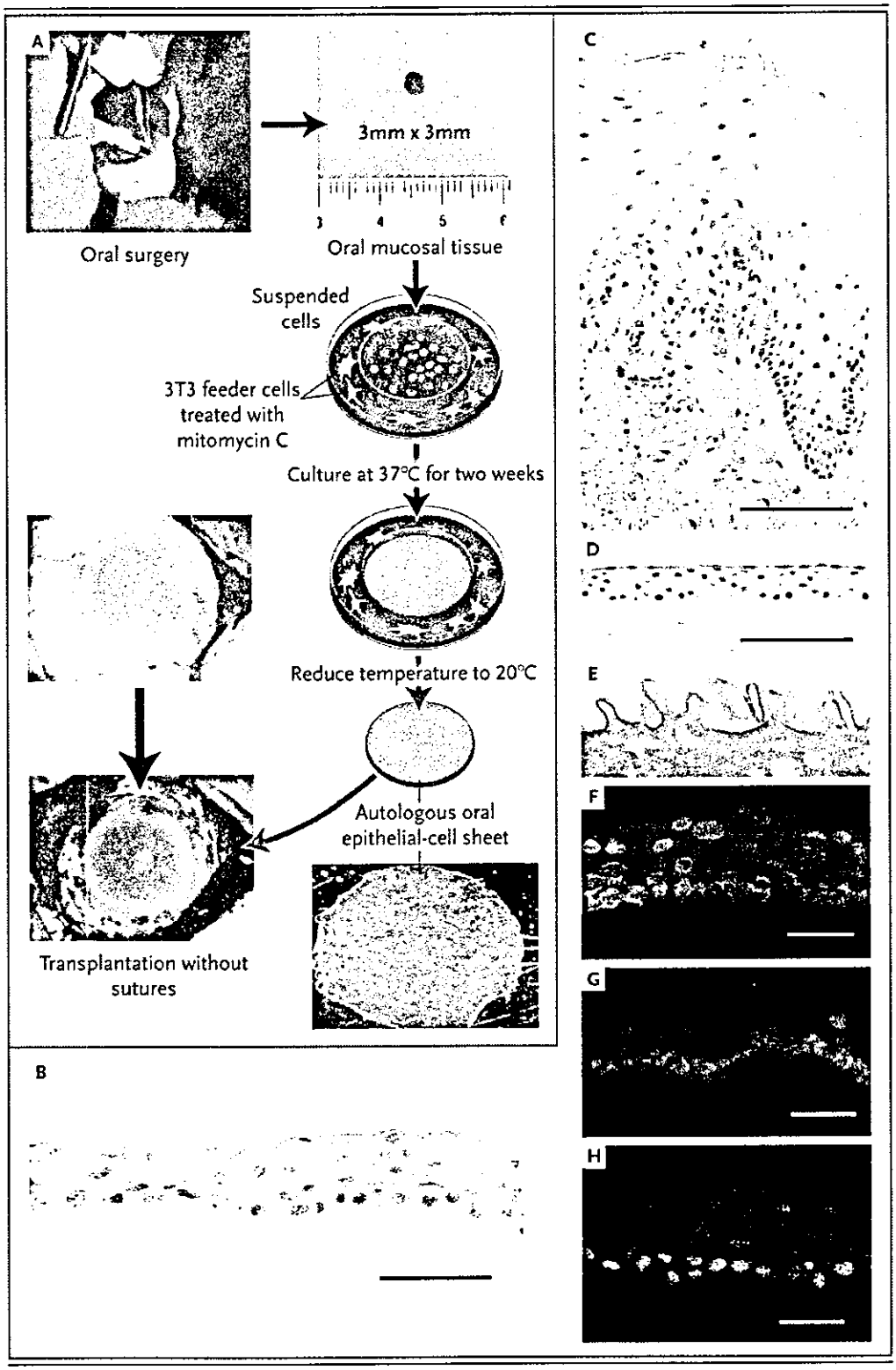
A
Oral surgery
3mm x 3mm
Oral mucosal tissue
Suspended cells
3T3 feeder cells treated with mitomycin C
Culture at 37°C for two weeks
Reduce temperature to 20°C
Autologous oral epithelial-cell sheet
Transplantation without sutures
B
C
D
E
F
G
H

IMMUNOHISTOLOGY

Cryosections from cell sheets were immunostained with monoclonal anti–keratin 3 antibodies (AE5, Progen Biotechnik), anti–β_1 integrin antibodies (P5D2, Santa Cruz Biotechnology), or anti-p63 antibodies (4A4, Santa Cruz Biotechnology) and fluorescein isothiocyanate–labeled or rhodamine-labeled secondary antibodies (Jackson ImmunoResearch Laboratories). Nuclei were costained with Hoechst 33342 (Molecular Probes) or propidium iodide (Sigma). Stained cells were observed using confocal laser scanning microscopy (LSM-510, Zeiss). The same concentration of corresponding normal nonspecific IgG provided negative controls, and native human corneal and limbal tissues were used as positive controls.

TRANSPLANTATION OF CELL SHEETS TO THE EYE

We removed the conjunctival and subconjunctival scar tissue from the cornea up to 3 mm outside the limbus to reexpose corneal stroma (Fig. 2, and a video clip in the Supplementary Appendix, available with the full text of this article at www.nejm.org). Subsequently, the harvested sheet of autologous oral mucosal epithelial cells was placed directly onto the exposed transparent stromal bed as described previously.[6,23] No sutures were required. The grafted corneal surface was then covered with a soft contact lens for protection during healing. After surgery, topical antibiotics (0.3 percent ofloxacin) and steroids (0.1 percent betamethasone) were initially applied four times a day and then tapered to three times a day. During the first week after surgery, betamethasone (1 mg per day) was administered orally to reduce postoperative inflammation. One month after surgery, the administration of topical corticosteroids was changed from 0.1 percent betamethasone to 0.1 percent fluorometholone. Because the patients had severe dry eye, proper wound healing could not be expected without tear supplementation. Preservative-free artificial tears were frequently used, and the puncta lacrimale of all the patients were occluded to increase tear retention.

RESULTS

CHARACTERIZATION OF TISSUE-ENGINEERED EPITHELIAL-CELL SHEETS

We compared cultured autologous oral mucosal-cell sheets with endogenous tissue both functionally and phenotypically. Oral mucosal epithelial cells cultured under these culture conditions resemble corneal epithelium, with three to five cell layers, small basal cells, flattened middle cells, and polygonal and flattened superficial cells (Fig. 1B), more than they resemble native oral mucosal epithelium (Fig. 1C), which is much thicker than corneal epithelium (Fig. 1D). The optical transparency of harvested cell sheets was equal to that of corneal epithelial-cell sheets originating from limbal stem cells (data not shown).[23]

Ultrastructural examination revealed an architecture of well-structured, compact, multilayered cell sheets with the expected microstructures of the native cells, including microvilli (Fig. 1E), tight junctions, desmosomes, and basement membrane. Such morphologic characteristics are similar to those of corneal epithelium in vivo. Native corneal epithelial cells and oral mucosal epithelial cells express keratin 3 as a characteristic phenotypic marker, and harvested epithelial-cell sheets also express keratin 3 (Fig. 1F).

The mean (±SE) colony-forming efficiency, calculated as the ratio of the number of stem or progenitor cells that can produce colonies to the total number of cells in the harvested tissue, was 2.1±0.9 percent for all four patients (with measurements performed in triplicate in each patient), confirming the presence of progenitor cells among the isolated oral mucosal epithelial cells. Correspondingly, β_1 integrin, reported to be an epithelial stem-cell and progenitor-cell marker[24] susceptible to digestion by trypsin, remained intact in the basal cells (Fig. 1G). The basal cells in the multilayered cell sheets also express p63 (Fig. 1H), a putative epithelial stem-cell marker.[25]

CLINICAL RESULTS OF TRANSPLANTATION OF THE CELL SHEET TO THE CORNEAL SURFACE

Attachment of the cell sheet to the stromal bed was spontaneous and uniform (Fig. 2, and video clip in the Supplementary Appendix). Within several minutes after placement without sutures, the grafted cell sheets remained intact and stably bound to the stromal surfaces, even after the extensive application of eyedrops. This observation is consistent with previous experiments with rabbit models, in which transplanted sheets of oral mucosal epithelial cells readily resisted outward displacement when the perimeters were pulled with forceps.

Immediately after surgery, the transplanted corneal surface was clear and smooth, without observable vascularization. Within one week, slit-lamp ex-

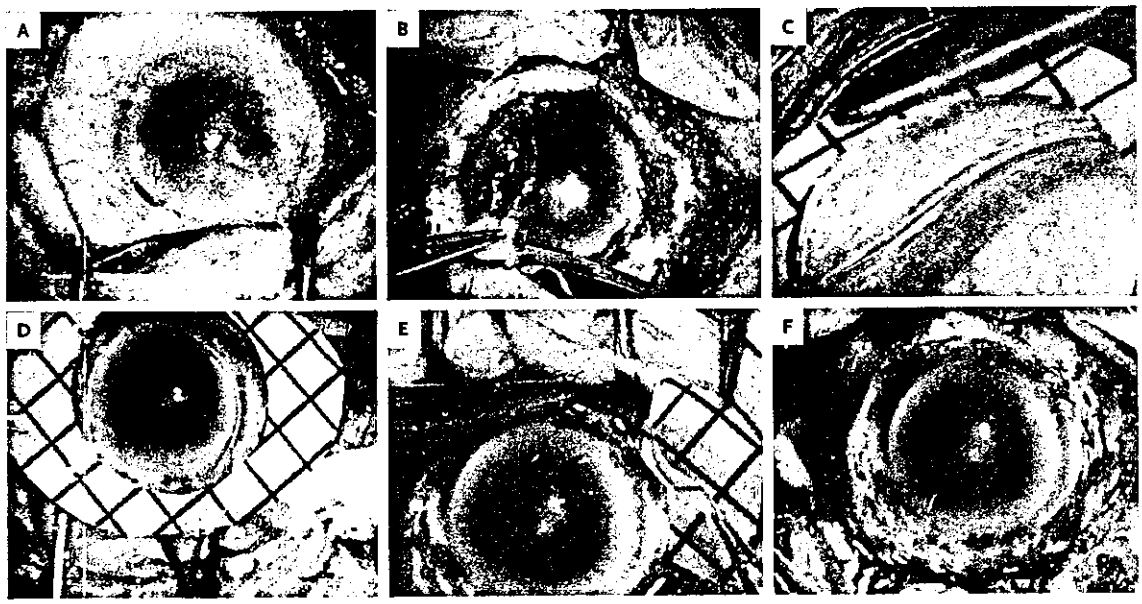

Figure 2. Transplantation Procedures for Tissue-Engineered Autologous Epithelial-Cell Sheets.

Preoperatively, the entire corneal surface was covered by conjunctival tissue with neovascularization (Panel A). In Panel B, conjunctival tissue over the cornea is surgically removed to reexpose transparent corneal stroma. Then, the sheet of tissue-engineered epithelial cells is harvested from a temperature-responsive culture insert with the use of a doughnut-shaped supporter ([black-and-white squares] Panel C) and placed on the stromal bed (Panel D). The sheet adheres to corneal stroma in a few minutes without sutures, and the supporter is removed (Panel E), leaving the cell sheet on the stroma (Panel F). A video clip can be viewed in the Supplementary Appendix, available with the full text of this article at www.nejm.org.

amination with fluorescein sodium staining showed complete reepithelialization of the corneal surface in all four eyes, revealing the tight junction–mediated barrier function. Corneal transparency was restored without any defects of the corneal epithelium. In all eyes, stromal vascularization gradually recurred in the peripheral cornea but not in the central zone. This vascularization was unlike subepithelial vascularization accompanied by conjunctival ingrowth, since it was localized to the deeper stroma and did not show the abnormally high fluorescein permeability characteristic of conjunctival epithelium.

During a mean follow-up period of 14 months, corneal transparency was maintained (Fig. 3 and Table 2). Maximally improved visual acuity was obtained 6, 2, 10, and 8 weeks after transplantation for Patients 1 through 4, respectively, and became stable thereafter. The length of time until visual acuity improved seemed to correspond to the length of time until the corneal stroma became less opaque. No complications were observed.

DISCUSSION

Our study shows that tissue-engineered cell sheets from autologous oral mucosal epithelium may serve as effective substitutes for allografts of limbal tissue in the reconstruction of the corneal and limbal surfaces. Four patients (four eyes) were consecutively treated with this approach, and corneal transparency was restored and postoperative visual acuity improved remarkably (Table 2). During the follow-up period, all corneal surfaces remained transparent, and there were no serious complications.

We developed this strategy on the basis of several observations from cell biology and medicine. First, in vivo oral mucosal epithelium expresses keratin 3, which is also expressed by the corneal epithelium but not by the epidermis.[1,27] Second, the excision of a small piece of oral mucosal tissue from the patient is straightforward, and the resulting wound heals within several days without incident or scarring. Third, transplantation of autologous

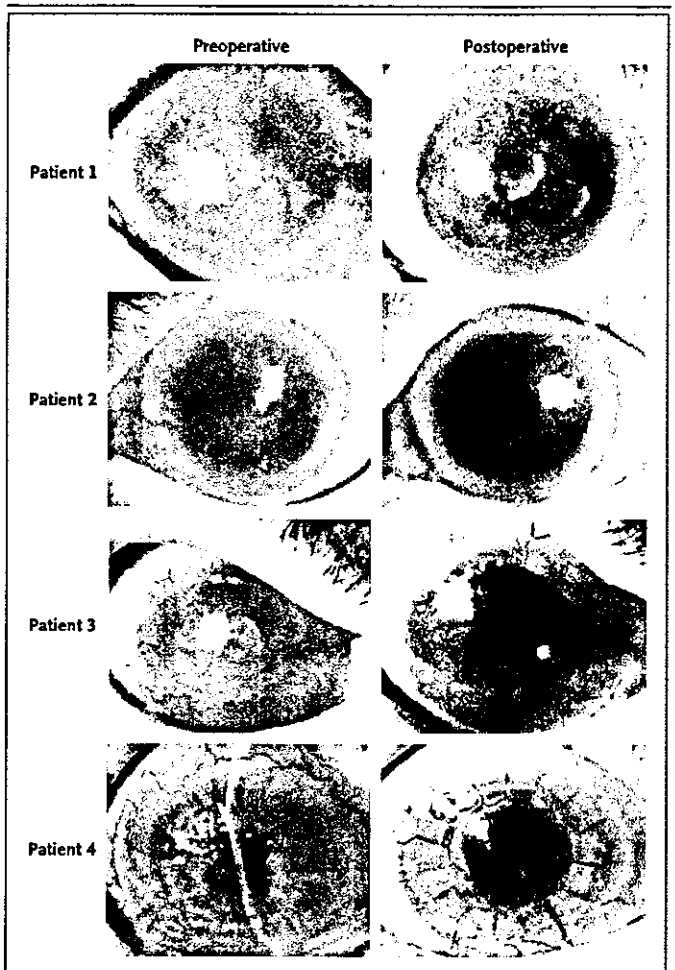

Figure 3. Eyes of Patients before and after Transplantation of Sheets of Tissue-Engineered Autologous Epithelial Cells.

These photographs were taken just before transplantation of the cell sheets and postoperatively at 13, 14, or 15 months.

buccal mucosal grafts directly onto ocular surfaces was previously reported in human patients[28] for the purposes of treating corneal ulcers, corneal perforations, and lid abnormalities (e.g., marginal entropion and trichiasis); these grafts are not useful for improving vision, since they contain opaque subepithelial fibrous tissue. In contrast, the transparency of carrier-free sheets of tissue-engineered epithelial cells fabricated from oral mucosal epithelial cells is similar to the transparency of corneal epithelial-cell sheets originating from limbal stem cells.[23]

Reconstruction with autologous oral mucosal epithelial cells offers substantial clinical advantages over allogeneic transplantation for treating severe diseases such as the Stevens–Johnson syndrome and ocular pemphigoid. It averts the risks of allogeneic immunorejection and immunosuppression. Severe tear-film and lid abnormalities often associated with these diseases continue to be a challenge, since immunologically driven inflammation of the ocular surface persists chronically in these patients.

Although decisive epithelial stem-cell markers that could provide evidence of the presence of these stem cells in grafted cell sheets have not yet been established,[29] results from colony-forming assays for oral mucosal epithelium show that excised oral tissue contains epithelial stem cells or at least progenitor cells. Since ocular surfaces that have been grafted with cell sheets retain their transparency for more than one year, and because the life spans of transient amplifying cells (cells committed to epithelial differentiation) are believed to be less than one year,[30] we conclude that progenitor cells with the potential to differentiate into new corneal epithelial phenotype are present in autografts of cell sheets.

Conjunctival epithelial cells invade the cornea after allogeneic transplantation because of the gradual depletion of allogeneic corneal epithelial cells due to epithelial rejection or stem-cell depletion.[31-33] It is unknown whether this also applies to autologous transplants. In the four eyes we studied, limited stromal vascularization occurred within a few months after transplantation of the cell sheet and reached a stable state within six months, with no appreciable growth thereafter. This stromal vascularization was observed only beneath cell sheets on peripheral corneas and should be distinguished from the subepithelial neovascularization accompanied by conjunctival ingrowth that results from the stem-cell loss associated with allografts, which occurs several months after transplantation. This finding suggests that grafted oral mucosal epithelial cells remained on the ocular surface.

It is possible that the reduction in host immunologic reactions associated with the grafting of autologous cells may minimize epithelial rejection, but further study is needed. The limited stromal neovascularization that we observed is probably caused by angiogenic factors secreted from tissue-engineered epithelial-cell sheets fabricated from oral mucosal epithelial cells originally located in

Table 2. Surgical Outcome in Four Patients Who Received Transplants of Tissue-Engineered Autologous Oral Mucosal-Cell Sheets.

Patient No.	Best Corrected Visual Acuity in Damaged Eye		Corneal Opacity (Grade)*			Complication	Months of Follow-up
	Preoperative†	Postoperative	Preoperative	1 Month after Surgery	At Last Observation		
1	Counting fingers	20/100	3	2	1	None	15
2	20/2000	20/25	3	1	1	None	14
3	Hand motion	20/300	3	1	1	None	14
4	20/2000	20/50	3	1	1	None	13

* The extent of corneal opacity was graded by three masked observers on the basis of the slit-lamp examination with a previously described system[26] and modifications for ocular-surface diseases. Grade 0 indicates clear or trace haze, grade 1 mild opacity, grade 2 moderately dense opacity partially obscuring details of the iris, and grade 3 severely dense opacity obscuring details of the intraocular structure. Grading is based on the opacity observed in all corneal layers, including epithelium, stroma, and endothelium.

† The visual acuity of patients who could not read a visual-acuity chart at a distance of 0.5 m was assessed by asking whether they could see the number of fingers held up by the examiner. If they could not, visual acuity was assessed by the patient's ability to see hand movement by the examiner.

vivo on the substantia propria, which is rich in vessels. However, the production of antiangiogenic factors such as thrombospondin by keratocytes[34] may limit vascularization to peripheral areas.

We observed that the transplanted cell sheets became more transparent and achieved smoother, integrated surfaces on the corneal stroma, further resembling normal corneal epithelium; a plateau was reached one to three months after transplantation. Originally, oral mucosal epithelium, located on substantia propria, is morphologically distinct from corneal epithelium in that it is much thicker and multilayered and has an irregular surface (Fig. 1C). The use of temperature-responsive harvesting allows the grafted carrier-free oral mucosal epithelial cells to interact immediately and directly with patients' corneal stromal keratocytes without interference from cell carriers such as fibrin gel and amniotic membranes.

Our transplantable epithelial-cell sheets used the common 3T3 feeder-layer method originally developed for the production of autologous epidermal-cell grafts[35] and used in the culture of other epithelial cells from various tissue sources, including the limbus.[16] This method has been clinically applied since the 1980s for the treatment of various skin conditions, including burns and giant nevi, although the Food and Drug Administration classifies these grafts as xenografts.

In summary, we have shown that sheets of tissue-engineered epithelial cells fabricated ex vivo from autologous oral mucosal epithelium are effective for reconstructing the ocular surface and restoring vision in patients with bilateral total stem-cell deficiencies. Long-term follow-up and experience with a large series of patients are needed to assess further the benefits and risks of this method, which offers the potential to treat severe ocular diseases that are resistant to standard approaches.

Supported by Grants-in-Aid for Scientific Research (15390530, 16200036, and 16300161), the High-Tech Research Center Program, and the Center of Excellence Program for the 21st Century from the Ministry of Education, Culture, Sports, Science, and Technology in Japan and by the Core Research for Evolution Science and Technology from the Japan Science and Technology Agency.

We are indebted to Professor David Grainger, Colorado State University, and Mr. Joseph Yang, Tokyo Women's Medical University, for their technical review.

REFERENCES

1. Schermer A, Galvin S, Sun TT. Differentiation-related expression of a major 64K corneal keratin in vivo and in culture suggests limbal location of corneal epithelial stem cells. J Cell Biol 1986;103:49-62.
2. Cotsarelis G, Cheng SZ, Dong G, Sun TT, Lavker RM. Existence of slow-cycling limbal epithelial basal cells that can be preferentially stimulated to proliferate: implications on epithelial stem cells. Cell 1989;57:201-9.
3. Thoft RA, Friend J. The X, Y, Z hypothesis of corneal epithelial maintenance. Invest Ophthalmol Vis Sci 1983;24:1442-3.
4. Buck RC. Measurement of centripetal migration of normal corneal epithelial cells in the mouse. Invest Ophthalmol Vis Sci 1985; 26:1296-9.
5. Tseng SC. Concept and application of limbal stem cells. Eye 1989;3:141-57.
6. Nishida K. Tissue engineering of the cornea. Cornea 2003;22:Suppl 7:S28-S34.

7. Kenyon KR, Tseng SC. Limbal autograft transplantation for ocular surface disorders. Ophthalmology 1989;96:709-22.
8. Chen JJ, Tseng SC. Corneal epithelial wound healing in partial limbal deficiency. Invest Ophthalmol Vis Sci 1990;31:1301-14.
9. Dua HS, Azuara-Blanco A. Autologous limbal transplantation in patients with unilateral corneal stem cell deficiency. Br J Ophthalmol 2000;84:273-8.
10. Tsubota K, Satake Y, Kaido M, et al. Treatment of severe ocular-surface disorders with corneal epithelial stem-cell transplantation. N Engl J Med 1999;340:1697-703.
11. Samson CM, Nduaguba C, Baltatzis S, Foster CS. Limbal stem cell transplantation in chronic inflammatory eye disease. Ophthalmology 2002;109:862-8.
12. Ilari L, Daya SM. Long-term outcomes of keratolimbal allograft for the treatment of severe ocular surface disorders. Ophthalmology 2002;109:1278-84.
13. Shimazaki J, Shimmura S, Fujishima H, Tsubota K. Association of preoperative tear function with surgical outcome in severe Stevens-Johnson syndrome. Ophthalmology 2000;107:1518-23.
14. Schwab IR, Reyes M, Isseroff RR. Successful transplantation of bioengineered tissue replacements in patients with ocular surface disease. Cornea 2000;19:421-6.
15. Tsai RJ, Li LM, Chen JK. Reconstruction of damaged corneas by transplantation of autologous limbal epithelial cells. N Engl J Med 2000;343:86-93.
16. Rama P, Bonini S, Lambiase A, et al. Autologous fibrin-cultured limbal stem cells permanently restore the corneal surface of patients with total limbal stem cell deficiency. Transplantation 2001;72:1478-85.
17. Nakamura T, Endo K, Cooper LJ, et al. The successful culture and autologous transplantation of rabbit oral mucosal epithelial cells on amniotic membrane. Invest Ophthalmol Vis Sci 2003;44:106-16.
18. Kinoshita S, Nakamura T. Development of cultivated mucosal epithelial sheet transplantation for ocular surface reconstruction. Artif Organs 2004;28:22-7.
19. Yamato M, Okano T. Cell sheet engineering. Mater Today 2004;May:42-7.
20. Kawasaki S, Nishida K, Sotozono C, Quantock AJ, Kinoshita S. Conjunctival inflammation in the chronic phase of Stevens-Johnson syndrome. Br J Ophthalmol 2000;84:1191-3.
21. Foster CS, Fong LP, Azar D, Kenyon KR. Episodic conjunctival inflammation after Stevens-Johnson syndrome. Ophthalmology 1988;95:453-62.
22. Hirose M, Kwon OH, Yamato M, Kikuchi A, Okano T. Creation of designed shape cell sheets that are noninvasively harvested and moved onto another surface. Biomacromolecules 2000;1:377-81.
23. Nishida K, Yamato M, Hayashida Y, et al. Functional bioengineered corneal epithelial sheet grafts from corneal stem cells expanded ex vivo on a temperature-responsive cell culture surface. Transplantation 2004;77:379-85.
24. Jones PH, Watt FM. Separation of human epidermal stem cells from transit amplifying cells on the basis of differences in integrin function and expression. Cell 1993;73:713-24.
25. Pellegrini G, Dellambra E, Golisano O, et al. p63 Identifies keratinocyte stem cells. Proc Natl Acad Sci U S A 2001;98:3156-61.
26. Fantes FE, Hanna K, Waring GO III, Pouliquen Y, Thompson KP, Salvodelli M. Wound healing after excimer laser keratomileusis (photorefractive keratectomy) in monkeys. Arch Ophthalmol 1990;108:665-75.
27. Moll R, Franke WW, Schiller DL, Geiger B, Krepler R. The catalog of human cytokeratins: patterns of expression in normal epithelia, tumors and cultured cells. Cell 1982;31:11-24.
28. Shore JW, Foster CS, Westfall CT, Rubin PA. Results of buccal mucosal grafting for patients with medically controlled ocular cicatricial pemphigoid. Ophthalmology 1992;99:383-95.
29. Dua HS, Joseph A, Shanmuganathan VA, Jones RE. Stem cell differentiation and the effects of deficiency. Eye 2003;17:877-85.
30. Kinoshita S, Friend J, Thoft RA. Sex chromatin of donor corneal epithelium in rabbits. Invest Ophthalmol Vis Sci 1981;21:434-41.
31. Holland EJ, Schwartz GS. Epithelial stem-cell transplantation for severe ocular-surface disease. N Engl J Med 1999;340:1752-3.
32. Shimazaki J, Kaido M, Shinozaki N, et al. Evidence of long-term survival of donor-derived cells after limbal allograft transplantation. Invest Ophthalmol Vis Sci 1999;40:1664-8.
33. Williams KA, Brereton HM, Aggarwal R, et al. Use of DNA polymorphisms and the polymerase chain reaction to examine the survival of a human limbal stem cell allograft. Am J Ophthalmol 1995;120:342-50.
34. Hiscott P, Sorokin L, Nagy ZZ, Schlotzer-Schrehardt U, Naumann GO. Keratocytes produce thrombospondin 1: evidence for cell phenotype-associated synthesis. Exp Cell Res 1996;226:140-6.
35. Rheinwald JG, Green H. Serial cultivation of strains of human epidermal keratinocytes: the formation of keratinizing colonies from single cells. Cell 1975;6:331-43.

POSTING PRESENTATIONS AT MEDICAL MEETINGS ON THE INTERNET

Posting an audio recording of an oral presentation at a medical meeting on the Internet, with selected slides from the presentation, will not be considered prior publication. This will allow students and physicians who are unable to attend the meeting to hear the presentation and view the slides. If there are any questions about this policy, authors should feel free to call the *Journal*'s Editorial Offices.

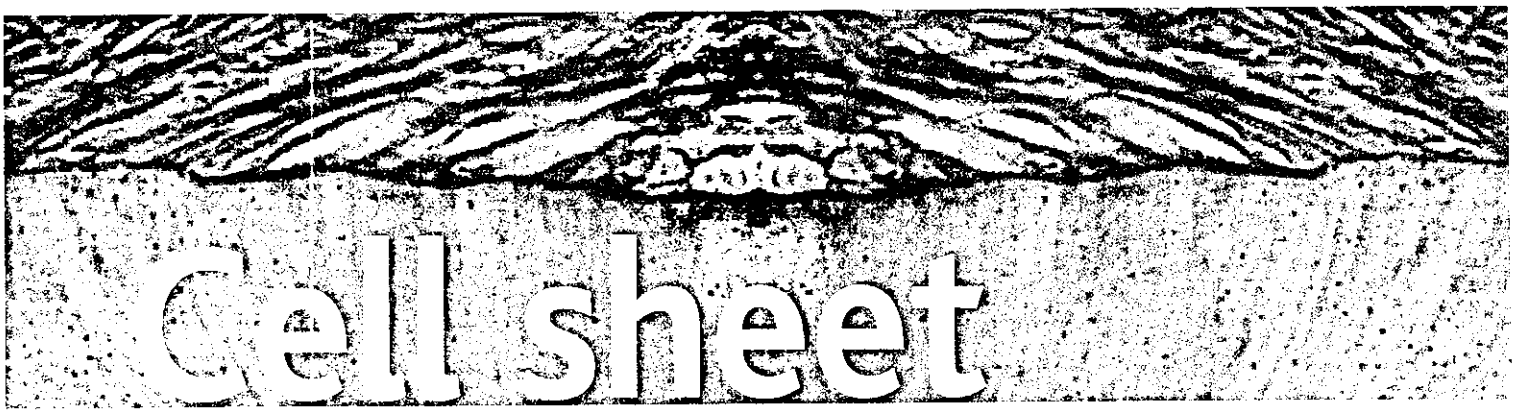

Cell sheet engineering

by Masayuki Yamato and Teruo Okano

We have developed 'cell sheet engineering' in order to avoid the limitations of tissue reconstruction using biodegradable scaffolds or single cell suspension injection. Our concept is tissue reconstruction, not from single cells, but from cell sheets. Cell sheets are prepared using temperature-responsive culture dishes. Temperature-responsive polymers are covalently grafted onto the dishes, allowing various types of cells to adhere and proliferate at 37°C. The cells spontaneously detach when the temperature is reduced below 32°C without the need for proteolytic enzymes. The confluent cells are noninvasively harvested as single, contiguous cell sheets with intact cell-cell junctions and deposited extracellular matrix (ECM). We have used these harvested cell sheets for various tissue reconstructions, including ocular surfaces, periodontal ligaments, cardiac patches, and bladder augmentation.

Institute of Advanced Biomedical Engineering and Science,
Tokyo Women's Medical University,
8-1 Kawada-cho,
Shinjuku-ku,
Tokyo 162-8666, Japan
E-mail: tokano@abmes.twmu.ac.jp

In the 21st century, novel therapeutics will be established. Controlled drug delivery has already been commercialized for limited uses. Gene therapy in human patients is being investigated experimentally. Furthermore, robotic surgery systems, as well as computer-aided surgery navigation systems, are commercially available. Tissue engineering was first proposed in the 1980s by a chemist, R. Langer, and a surgeon, J. P. Vacanti[1]. The key technology is the use of biodegradable polymer scaffolds, preformed in the target tissue shape, for cell seeding[2], as demonstrated in the well-publicized reconstruction of cartilage tissues for the growth of human ears on mice. By combining preformed biodegradable polymer scaffolds and specific cell types, various tissues including cartilage, bone, and blood vessels have been reconstructed, although, so far, therapeutic use has been very limited.

After transplantation of tissue-engineered constructs into hosts, the scaffolds degrade over weeks or months. The space formerly occupied by the scaffold is filled with proliferated cells and/or deposited ECM, such as collagen. However, ECM deposition in tissues often results in fibrosis, a pathological state. Furthermore, various properties of the scaffold can be undesirable in some tissues. For example, the opacity and inflexibility of polymer scaffolds inevitably impair

ISSN:1369 7021 © Elsevier Ltd 2004

ophthalmological and cardiac tissue reconstruction, respectively.

With the rapid progress in the understanding of stem cell biology during the 1990s, the clinical use of stem cells seems to be promising. Recently, novel therapeutics using tissue engineering and stem cell technology, termed regenerative medicine, have been investigated. In experimental transplantation into small animals, such as rats and mice, the injection of single cell suspensions sometimes works. However, single cell suspension injection does not seem to be suitable for large tissue reconstruction, since only a few percent of the injected cells are integrated into host tissues. It is apparent that we currently lack successful methods of tissue reconstruction. This is the reason why we have proposed 'cell sheet engineering'. As biodegradable polymers are the key technology in first-generation tissue engineering, we are developing temperature-responsive culture dishes for the next generation.

Temperature-responsive culture dishes

Histologically, parenchyma (tissue characteristic of an organ) comprise intimately associated cell sheets. For example, the liver comprises sheets of hepatocytes and endothelial cells that are interconnected to form a continuous three-dimensional tissue lattice. Cooperation between several types of cell sheets has been revealed to be essential in tissue functions that are damaged in pathological conditions. Such observations are also supported by developmental biology, since every organ originates from three different cell sheets called the endoderm, mesoderm, and ectoderm. The cell sheets interact with each other in the development of organs. These considerations have encouraged us to initiate cell-sheet-based tissue reconstruction.

Conventionally, cells are harvested using proteolytic enzymes such as trypsin and dispase. These enzymes degrade cell adhesion molecules and the deposited ECM to detach cultured cells. But at the same time, cell-cell junction proteins, as well as receptor proteins expressed on the cell membrane, are often damaged. Harvest of cultured cell sheets, therefore, is only achieved with exceptional cell types whose cell-cell junctions are less susceptible to such enzymes. In order to solve this problem, we first developed temperature-responsive culture dishes[3]. A temperature-responsive polymer, poly(*N*-isopropylacrylamide), is covalently grafted onto a culture dish surface. A grafted polymer layer of ~20 nm thickness allows control of temperature-responsive cell adhesion/detachment (Fig. 1). At 37°C, the surface is relatively hydrophobic, similar to commercially available tissue culture dishes, but becomes hydrophilic below 32°C. Various cell types adhere, spread, and proliferate on the surface at 37°C. On reducing the temperature to below 32°C, cells spontaneously lift up from the surface without the need for trypsin. Highly trypsin-susceptible cells, such as hepatocytes[4] and glial cells[5] retain their differentiated native cell functions after this noninvasive cell harvest.

Confluent cells are recovered as a single contiguous cell sheet with intact cell-cell junctions and deposited

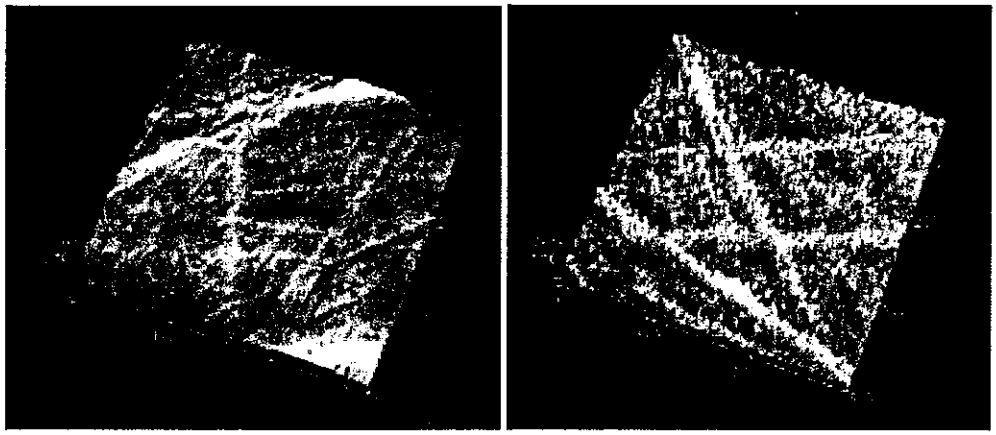

Fig. 1 Atomic force microscope images of temperature-responsive culture dish surfaces. Nongrafted, polystyrene culture dish surfaces (left) and poly(N-isopropylacrylamide)-grafted culture dish surfaces (right) were examined in air. Defects and scratches were observed on both surfaces. Small prickles can be seen on the grafted surface. Image size is 3 μm x 3 μm. Height is 25 nm (left) and 30 nm (right).